Localized Scale Coupling and New Educational Paradigms in Multiscale Mathematics and Science

Multiscale Mathematics Research and Education
Office of Science

US Department of Energy (DOE) grant DE-FG02-05ER25705
Final Report

Participants

- Los Alamos National Laboratory:
  - Alan Graham, Principal Investigator
  - Tony Redondo
- Sandia National Laboratories:
  - Lisa Mondy
  - Randy Schunk
  - Frank van Swol
- The University of New Mexico:
  - Marc Ingber
  - Peter Vorobieff
  - Marina Popova
- University of California, Santa Barbara:
  - L. Gary Leal

1. Introduction

The analysis of particles suspended in nonlinear, viscous shear flows is playing an increasingly important and often critical role in a number of developing technologies, including

- Processing of fibber-reinforced composites, encapsulants, and energetic materials
- Secondary oil recovery by hydraulic fracturing and CO_2 sequestration
- Well completion
- Transport of sediments, contaminants, and slurries
- Deburring and polishing of machine parts
- Chromatography (materials separation)
- Treatment of nuclear sludges

A major outstanding research issue that must be addressed to achieve progress in all these technologies is the elucidation of the relationships between the macroscopic system behavior (for example, where will the particles in shear flow migrate) and the flow microstructure. This issue cannot be addressed head-on either computationally or analytically, and instead requires a combination of approaches on different scales.

The reasons why the head-on approach is not feasible are as follows. In numerical modeling, any combined first-principles model using no *a priori* knowledge must resolve all the physically relevant scales. Sadly, the range of such relevant scales for particle-suspension flows is gigantic, because the largest scale is dictated by the scale of the system of interest (which can be hundreds of meters in any applications), while the smallest scale where most of the forces relevant for interaction of particles (e.g., van der Waals force) is literally molecular. Incorporating all these scales into a single model would be computationally prohibitive. From the

analytical point of view, the challenge is presented by the fact than on different scales, different physical mechanisms are dominant.

Additionally, a comprehensive approach must lead to useful practical results in terms of predicting the flows of interest, which means that a harmony must be achieved between analytical and numerical descriptions of particle-suspension flows, and experimental validation and verification must be conducted to ensure that the relevant physics are faithfully captured.

Thus a four-component approach to the problem was suggested (Fig. 1).

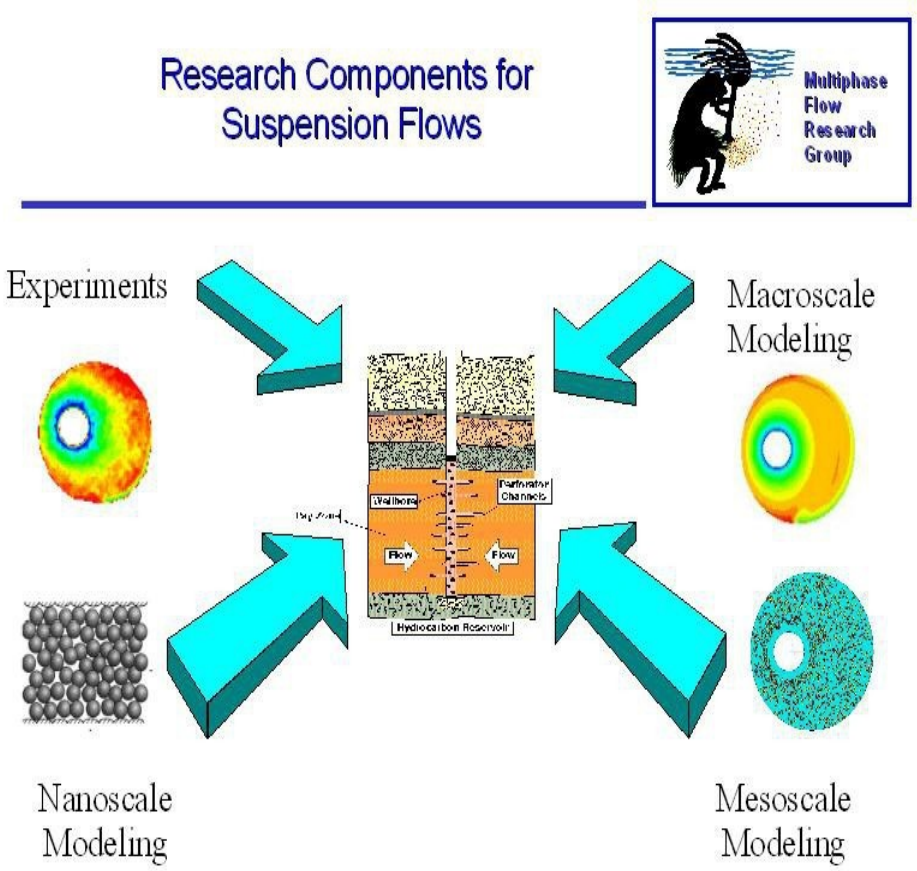

Figure 1. Schematic of the four research components for a study of suspension flows.

Modeling would be conducted on three distinct scales (macroscale, mesoscale, and nanoscale) and validated with experiments. Figure 2 additionally elucidates the three scales of the problem $d << \lambda << l$. The microscale d is bounded from above by the representative particle size and can go down all the way to molecular level. The mesoscale λ should represent a flow element containing enough particles to constitute a representative volume element (RVE). Finally, the macroscale models (scale l being representative of the size of the system) must represent the effects of the interaction of millions (or more) of particles without a need to track every individual particle.

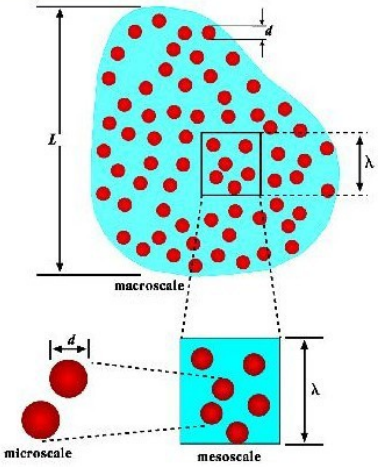

Figure 2. Macro-, meso-, and microscales in suspension flows.

On the largest (continuum-level) scale, the flow can be modeled with finite-element methods (FEM) with parallel implementation. On the mesoscale and down to particle-level scale, boundary-element methods (BEM) should be used, with lubrication correction to account for nearly-singular behavior in the case of touching or nearly touching particles. To resolve smaller relevant scales, molecular dynamics (MD) or dissipative particle dynamics (DPD) should be

applied.

Experimental results appropriate for verification and validation should also be scale-dependent. On the continuum level, particle-suspension behavior must be characterized with methods allowing to resolve particle group motion and local volume fraction without resolving individual particles. Among suitable methods for this approach is nuclear magnetic resonance (NMR) imaging. Particle interactions within a representative volume element can be tracked optically. On the microscale, atomic-force microscopy (AFM), interfacial-force microscopy (IFM), and other characterization methods can be used.

Based on this framework, our findings in this report are organized as follows. We begin with a description of the key experimental results, then describe the numerical work, and finally outline the most important physical conclusions, also describing the dissemination of our work and the follow-up research.

2. Experimental studies

Within the framework presented in the preceding section, the experiments described below can be characterized as investigations of phenomena relevant from the microscale to the mesoscale (Sections 2.1 and 2.2), or from the mesoscale to the macroscale (Section 2.2).

2.1. Experiments with particles in shear flow

Fundamentally, the simplest particle interaction that can occur in shear flow is between two particles brought together by the flow. This interaction also adds a surprising degree of complexity to the flow. The reason for that can be explained thus. For a particle size d, the

representative Reynolds number is $Re_d=Ud/\nu$, where U is flow velocity and ν is kinematic viscosity of the fluid. For a sufficiently small d, $Re_d << 1$, meaning that for the hydrodynamic part of the flow, Stokes approximation can be used, describing the fluid motion with equations that are time-reversible and much easier to solve than the full Navier-Stokes equations. This approach, however, will work without any additional complications only for a dilute suspension of particles. The moment particles come into contact, microscale-driven irreversibility enters the flow through boundary conditions, and the simplest case of a particle interaction involves just two particles. Moreover, this simplest situation also provides an excellent case for direct influence of microscale physics that govern the contact interaction due to surface roughness, solvation, and other forces upon the mesoscale flow (behavior of particles brought into contact).

We have conducted a careful experimental investigation of the behavior of two particles in shear flow that clearly shows that two-particle interaction is irreversible, with even nearly spherical smooth particles (average roughness ~250 nm, or 10^{-4} of the particle radius), showing a measurable deviation from the initial positions in a nominally reversible, stably stratified shear flow, where the inner cylinder of a cylindrical Couette cell is slowly rotated by the same angle clockwise and counterclockwise, bringing two particles into interaction. Although the final positions of the particles can be predicted only in the statistical sense, the center of mass of the particle pair moves outward toward the low-shear-rate region of the flow field, indicating that particle migration can occur in two-particle systems (Popova et al., 2007).

Variation in these final positions is caused by differences in the microscopic properties of the particle surfaces in the immediate vicinity of the point of closest proximity between the surfaces. Thus the two-particle interaction in shear flow indeed reveals a direct relationship

between microscale phenomena near this point and the macroscale behavior of the flow, as manifested by the variation in the final positions of the particles. Moreover, the statistical properties of the microscale surface features are directly correlated with the statistics of the particle displacements after the interaction.

The experimental arrangement (Fig. 3) uses a computer-controlled stepper motor to rotate the inner cylinder of a Couette cell with the radius of the inner cylinder r_i = 5 cm and the radius of the outer cylinder r_o = 10 cm. The cell is 4 cm deep and filled with a stratified viscous fluid (water solution of $ZnCl_2$ and Triton X100 solvent). Thus the height to width ratio of the fluid-filled cross section of the cell is about 0.8. The refractive index of the fluid is 1.49, matching that of the acrylic block from which the outer cylinder of the cell is machined, to facilitate imaging of the side views of the cell. The density and stratification of the fluid are selected to render the polymethyl methacrylate (PMMA) particles used in experiment neutrally buoyant at a depth of 1 cm from the free surface of the fluid. At this depth, the fluid density equals the specific density of the particles (1.05).

The overall density difference sufficient to keep the particles in this layer of neutral buoyancy (and thus effectively limit the particle motion to two-dimensional) from top to bottom of the cell due to stable stratification being on the order of 1% of this nominal density. Variation in other properties of the fluid, including refractive index and viscosity, due to this density gradient is minimal, as checked with visualization and rheometer tests. The surface characteristics of each PMMA particle used in the experiments have been well characterized using a scanning electron microscope, which provides a map of surface nonuniformities for each individual particle (Fig. 4).

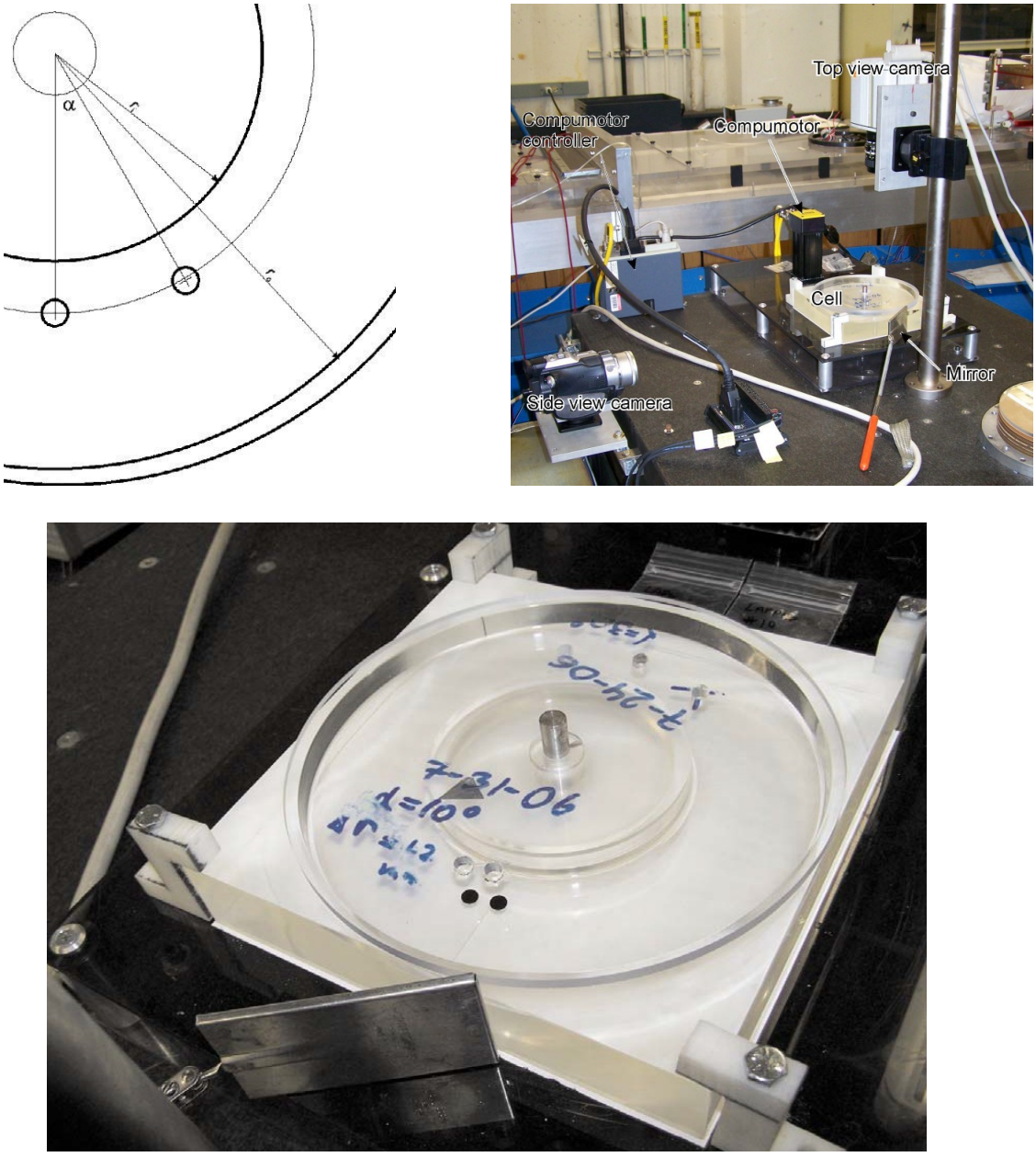

Figure 3. Experimental arrangement: geometric schematic (top left), the view of the arrangement (top right), and a closeup of the Couette cell (bottom) covered with one of the acrylic templates used to deposit the particles and the 45° mirror used to visualize particle movement in the horizontal plane at the bottom of the image.

“As is”

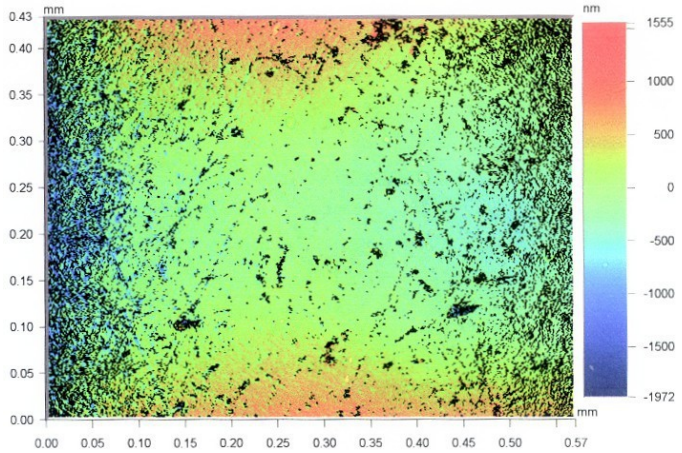

Diamond-lapped

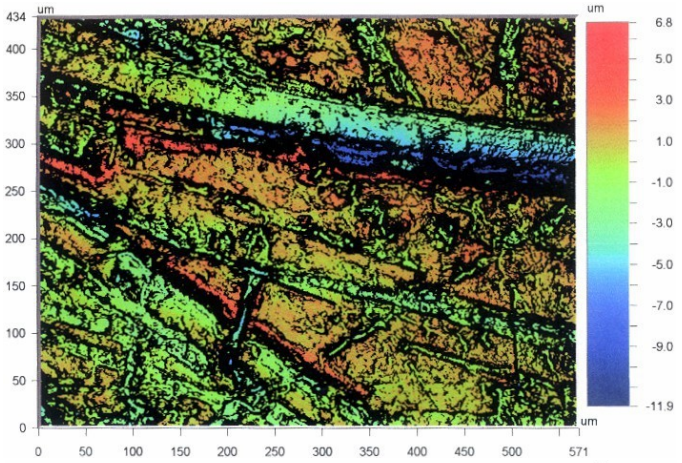

Bead-blasted

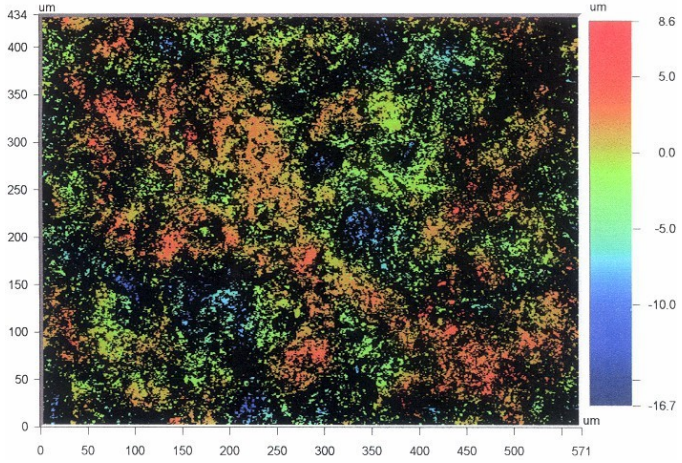

Figure 4. Maps of surfaces of particles used in experiments.

In the experiments, three different types of particles in terms of the surface treatment—original surface with the least roughness referred to as “smooth” in the subsequent paragraphs, lapped particles, and bead-blasted particles, the last type having the roughest surface. The goal of the experiment is to observe a two-particle interaction in a low-speed, nominally reversible shear flow, and to determine whether addition of the particles renders the flow irreversible, i.e., after the particles are positioned in the fluid and the inner cylinder of the Couette cell is rotated clockwise and then counterclockwise by the same angle, the particles do not return to their original positions after undergoing an interaction.

During experiments, a particle pair (nominal diameter d_p=0.635 cm) is positioned in the fluid by dropping the particles in through holes in a transparent cover over the Couette cell. This established a highly repeatable particle placement from experiment to experiment. Subsequently the particles settle in the fluid to a depth of 1 cm, where they reach neutral buoyancy. Then the inner cylinder is subjected to series of clockwise-counterclockwise rotations total angle 750°, with the top view camera capturing subsequent images of the particles after each rotation-counterrotation cycle. The positions of the particles in the horizontal plane are then converted to cylindrical coordinates (r, θ), using a computer program that calculates the centroid of each particle. This makes it possible to resolve the positions of the particles with a subpixel accuracy, the worst-case error not exceeding 0.3% of the particle diameter.

During each cycle of rotations, the particle pair can come into interaction twice: during the forward (clockwise) part of the cycle and during the counterclockwise (reverse) part. Comparison of the initial and final positions shows that, after this pair of interactions, the particles do not return to their initial positions. In the “reality check” experiments we conducted,

the particles were positioned in the Couette cell so that the rotation of the inner cylinder of the cell did not cause them to interact. In these experiments, we observed the particles return to their initial positions after the cell is rotated clockwise and then counter-clockwise with no discernible irreversibility.

In sheared particle-laden flows, the concentration of particles is known to change in the direction of the areas with minimal shear. The particle interaction in our experiments produces the same trend, as Fig. 5 shows.

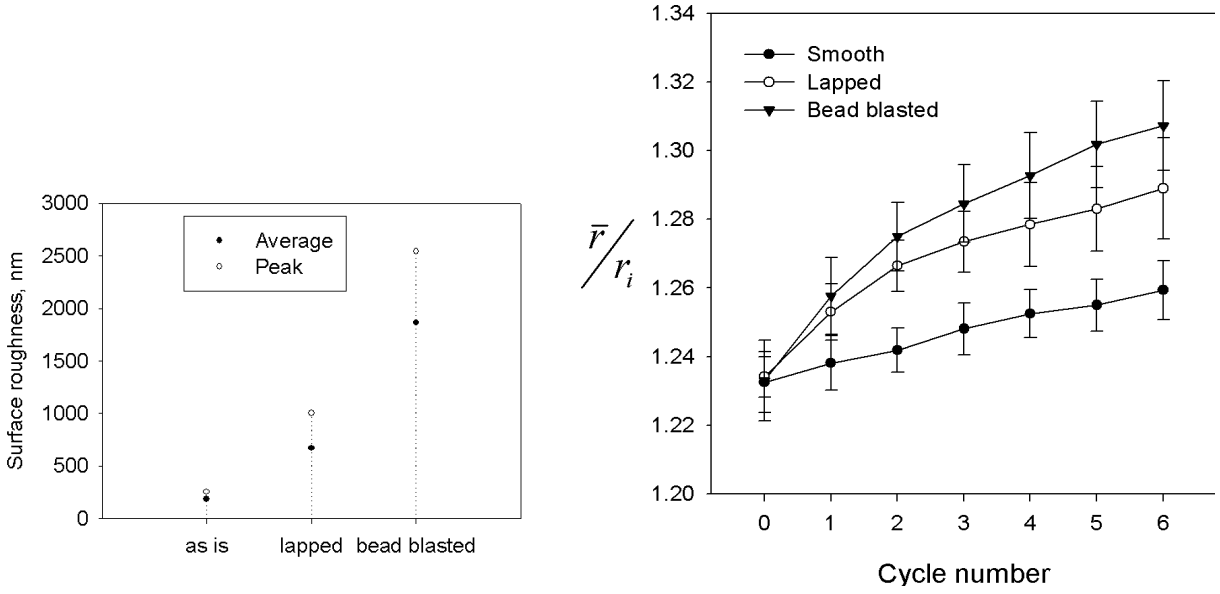

Figure 5. Left: average and maximum surface roughness of each type of particles used in experiment. Right: Evolution of the position of the center of mass of the system of two particles after six successive rotation/counterrotation cycles of 750°. 0 denotes the initial conditions; position is normalized by the radius of the rotating cylinder r_i.

This figure gives the initial radial positions of the center of mass of the two-particle system $(r_1+r_2)/2$, where $r_{1,2}$ are the initial distances of the centers of mass of the individual particles

from the center of the cell, as well as the corresponding distances after six rotation-counterrotation cycles. The data are averaged over ten experimental runs for each particle pair, with the error bars representing the standard deviation.

In all cases, there is a clear trend for the particles to move away from the rotating inner cylinder of the cell in the direction of lower shear. Thus one could argue that, in multiple-particle systems, two-particle interactions (and not more complicated multi-particle effects) already provide sufficient cause for the particles to migrate toward lower shear areas. The influence of the cylinder walls might affect this migration. We conducted some exploratory experiments where the particles were positioned further apart in the radial direction, so that the pair interaction was weaker. The main influence of the distance from the rotating inner cylinder was to alter the final radial spread of the two particles, with no statistically discernible effect on the final radial location of the center of mass.

It is also noteworthy and potentially useful that, while the particle pairs with all types of surface treatment (smooth, lapped, bead blasted) exhibit a similar trend in moving away from the higher-shear rate zone near the rotating inner cylinder, the extent of this radial motion appears to be related to the surface roughness, with the rougher particles exhibiting the most prominent movement. The error bars of the plots in Fig. 5 do not overlap; however, these plots can be collapsed by using an appropriate scaling of the radial coordinate *r*, namely

$$\hat{r} = \frac{r - r_{init}}{\sqrt{\delta_q / \delta_{q,sm}}}$$

where rinit is the initial position of the particle center (cycle 0 in Fig. 5), δ_q is the known maximum surface roughness, and $\delta_{q,sm}$ is the corresponding maximum roughness for the smooth

particles. This scaling is effectively a normalization of the radial displacement by the square root of the peak roughness. Figure 6 shows data of Figure 5 replotted with this scaling, demonstrating that the radial position plots indeed collapse.

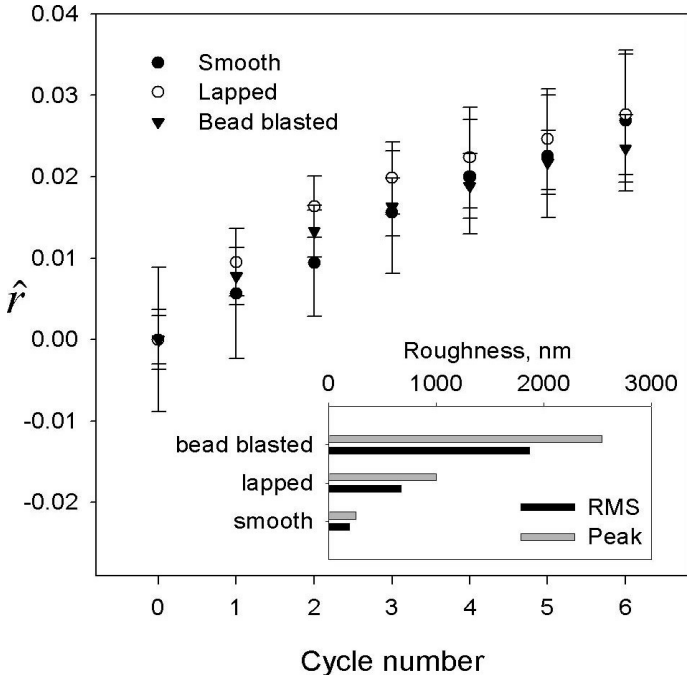

Figure 6. Positions of the center of mass of the system of two particles normalized by the square root of the peak surface roughness. The inset shows the peak and average (root mean square, labeled rms) roughness in nanometers for each particle type.

Based on the data presented above, a statistically relevant relationship exists between the extent of the irreversibility of the system comprised of two particles in shear flow and the surface properties of the particles. But can any interaction between multiple particles in a suspension be reduced to particle-pair interactions? It has been almost universally assumed in previous works that the most important interactions are those in particle pairs, with the force balance for a multi-particle system obtained as the sum of binary forces. This notion, however, was shown to be

theoretically incorrect for a dense configuration of particles. Thus another source of irreversibility due to nonlinear multi-particle interactions may exist in suspension flows. Its existence could account for the chaotic behaviour of the trajectories of *perfectly smooth* particles in numerical simulations of three-particle interactions in nominally reversible viscous flow, where any surface roughness–related irreversibility is eliminated in the numerical formulation of the problem.

To elucidate this issue, we conducted additional experiments using the same experimental arrangement, particles from the same sets, and the same fluid (Popova, Vorobieff, & Ingber, 2007). For the latter, we conducted rheometry measurements to obtain the kinematic viscosity $\nu = 146$ cm^2/s. The rheometry measurements also showed a linear relationship between torque and strain with no memory effects. Thus the fluid can be considered Newtonian (*i.e.*, shear stress in it is linearly proportional to the velocity gradient). The only difference from the earlier experiments was that now we used particle triplets instead of particle pairs. Now let us focus on the difference between two- and three particle interaction.

The initial conditions produced by the template as described in the preceding narrative have the particles nominally separated by 10° in the tangential (θ) direction. Between two particles in a pair, the initial difference in the radial distances is nominally 0.025 of the inner cylinder radius r_i. For the case of three particles, the initial radial distance increases by the same amount (0.025 r_i) between each particle. The velocity imparted by the rotation of the Couette cell to the particle closest to the inner cylinder is the highest, so it “catches up” to the next particle.

Figure 7 shows a superposition of images of a two-particle experiment, with the image on the left corresponding to the forward (clockwise) rotation of the inner cylinder and the image on

the right showing the reverse (counterclockwise) part of the cycle. Particle pairs in each sequence are labeled using the angle ϕ of the rotation of the inner cylinder, $\phi = 0$ corresponding to the initial and the final conditions. The "trailing" particle in the pair, initially positioned closer to the rotating cylinder, is marked with a white dot. In the second (counterclockwise rotation) picture, initial positions of the two particles are marked with contours. From the image sequence, it is clear that the close interaction of the two particles brings irreversibility to the flow, as we described earlier. The particles do not return to the initial positions.

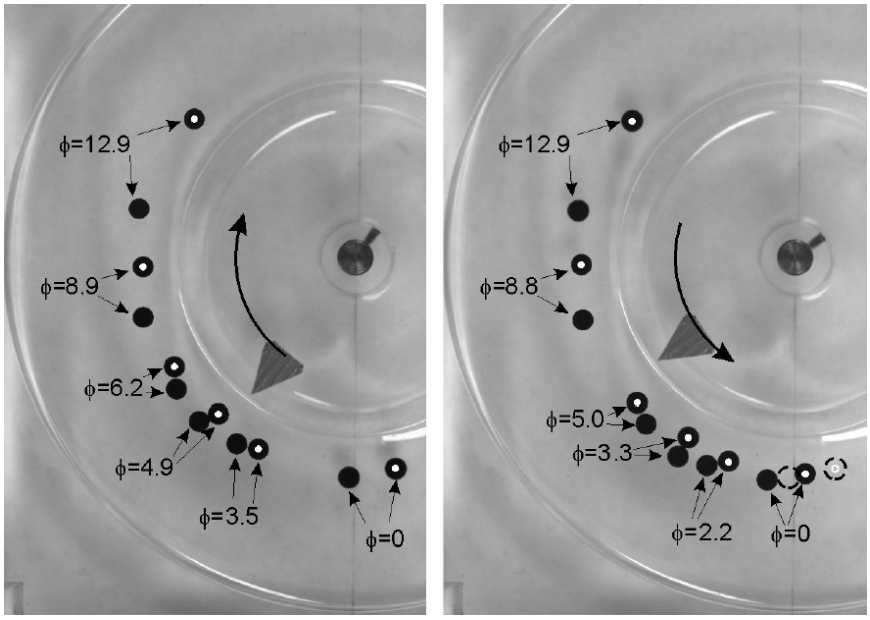

Figure 7. Forward (left) and reverse (right) parts of an experimental run with two particles. One of the particles is marked with a white dot for ease of identification (the dot is not physically present during the experiments). Values of the angle of rotation of the inner cylinder ϕ are shown for each particle pair. Dashed contours in the right image show the initial positions of the particles.

Moreover, the interactions themselves take place at different ranges of ϕ for the forward and reverse parts of the cycle: $3.5 < \phi < 6.2$ during clockwise rotation of the inner cylinder and $5.0 > \phi > 2.2$ during the counterclockwise rotation. This property of the interaction becomes even more apparent if the trajectories of the particles are plotted in the plane of polar coordinates (r, θ). Figure 8 shows such trajectories for two realizations of the experiment with different initial conditions, with the plot on the left corresponding to the image sequence of Fig. 7.

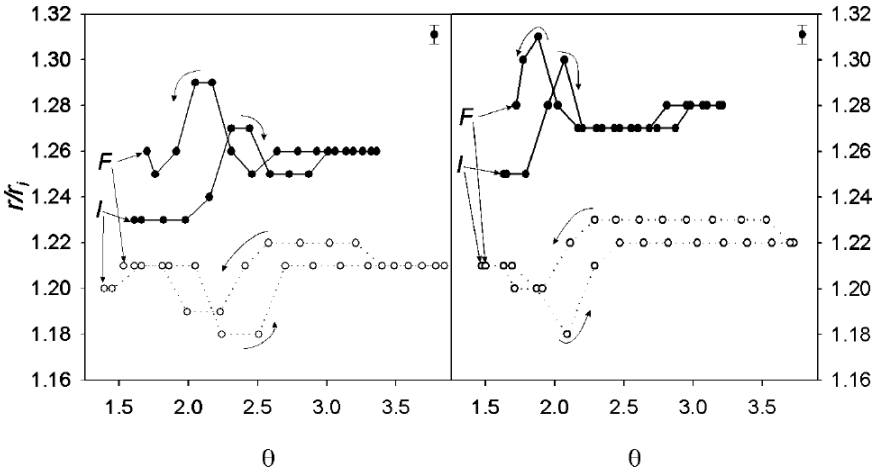

Figure 8. Polar coordinates (r, θ) of two particles during the forward-reverse cycle of the inner cylinder rotation. Plot on the left corresponds to Fig. 7, plot on the right was obtained from different initial conditions (greater initial distance from the inner cylinder). Representative error bars are in the upper right corner of each plot. Letters "I" and "F" denote the initial and final positions of the particles. Radius r is normalized by the inner cylinder radius r_i, angle θ is in radians, measured in the clockwise direction from a horizontal axis passing through the center of rotation.

While the particles do not return to their initial positions, their respective positions are retained (the "trailing" particle marked by the white dot in Fig. 7 returns to its "trailing" place

counterclockwise of the unmarked particle).

How does the addition of a third particle change the behavior of the system? Figure 9 shows a characteristic image sequence constructed in the same way as the sequence of Fig. 7, but with artificial markers now identifying the “middle” and the “trailing” particle, and the distance from the inner cylinder of the Couette cell increasing in the initial conditions from the “trailing” to the “middle” and to the “leading” (unmarked) particle.

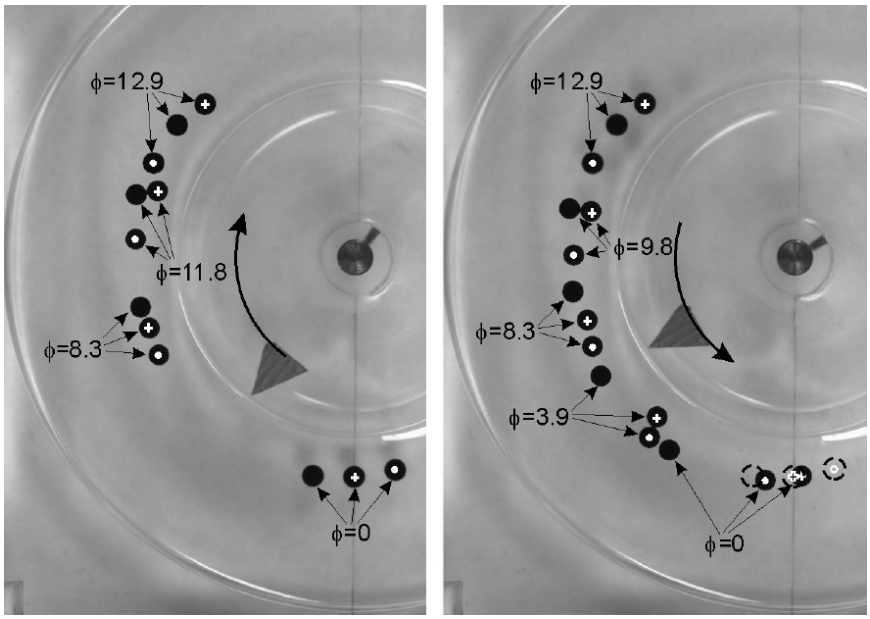

Figure 9. Forward (left) and reverse (right) parts of an experimental run with three particles. One particle (initially closest to the rotating cylinder) is marked with a white dot for ease of identification. The particle in the middle is marked with a “+” sign. The particle initially farthest from the rotating cylinder is unmarked. The marks are not physically present during the experiments. Values of the angle of rotation of the inner cylinder ϕ are shown for each particle triplet. Dashed contours in the right image show the initial positions of the particles.

There are several appreciable differences between the two- and three-particle cases. First, while the particles in a pair have a close interaction once during the forward and reverse parts of the cycle, particles in a triplet may have a different number of such encounters. In Fig. 7, the forward part of the cycle shows one such interaction beginning at $\phi = 8.3$. This interaction causes the "middle" and the "leading" particles to exchange their order with respect to the direction of rotation. A similar exchange takes place in Fig. 7.

However, during the reverse part of the three-particle experiment, two close approaches happen. The first one, occurring around $\phi = 8.8$, involves the "middle" and the "leading" particle again, with their initial order restoring itself . Then another close encounter happens, this time involving the "middle" and the "trailing" particle around $\phi = 3.9$. As the result, these two particles reverse their order in the θ coordinate direction. The initial order of the particles was "leading," "middle," "trailing." In Fig. 9, the final order of the particles is "leading," "trailing," "middle." Without detailed knowledge of the particle trajectories, it would not be possible to tell which one is which. In other words, three-particle interaction is not just irreversible, but chaotic. For additional elucidation of these features, Fig. 10 shows the particle trajectories in the (r, θ) plane for the experimental run depicted in Fig. 9.

As for the common features between the two- and three-particle cases, there exists a shared trend for the center of mass for the pair and the triplet to move away from the inner (rotating) cylinder of the cell. Moreover, the extent of this motion is related to the particle roughness, being the more pronounced, the rougher are the particles in the pair or triplet.

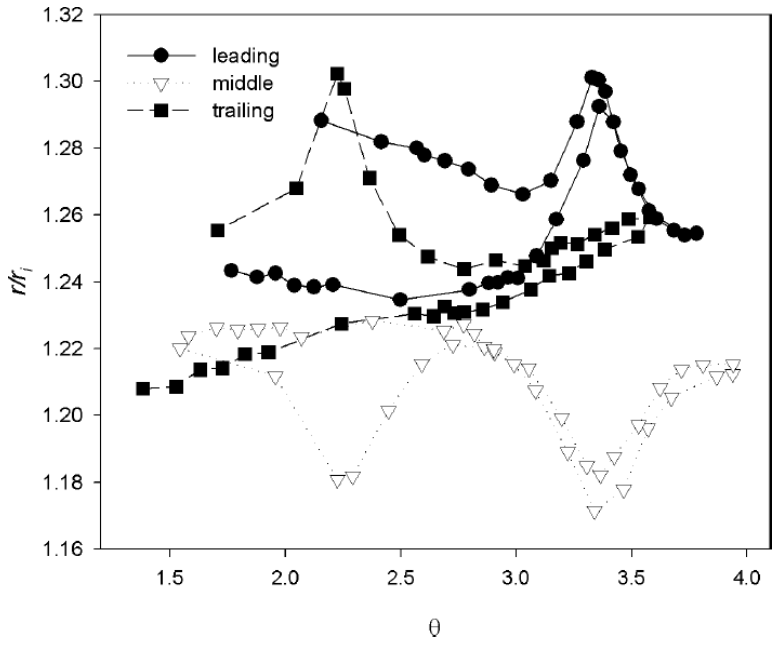

Figure 10. Polar coordinates (r, θ) of three particles during the forward-reverse cycle of the inner cylinder rotation. This plot corresponds to Fig. 9. Refer to the text for the description of the initial positions of the leading, middle, and trailing particle. Radius r is normalized by the inner cylinder radius r_i, angle θ is in radians, measured in the clockwise direction from a horizontal axis passing through the center of rotation.

2.2. Experiments with bubbles rising through suspensions of solid particles

The presence of bubbles in the flow adds an additional level of complexity. The characterization of the behavior of single bubbles rising in suspensions of solid particles is important to applications ranging from design of slurry bubble column reactors to flotation separation in minerals processing to degassing of filled polymers or ceramic precursors. Also, as the trend toward smaller geometries in both manufacturing and research continues, the need for a more thorough understanding of bubble rise in suspensions subject to smaller confining geometries

presents itself.

We conducted an experiment, where individual bubbles rising through suspensions of spherical particles neutrally buoyant in viscous Newtonian liquids are tracked with real time radiography. The effects of the containing cylinder, suspended particle, and bubble sizes were studied for particle volume fractions ranging from 0.20 to 0.50 (Mondy et al., 2008).

Figure 11 shows a sketch of the experimental setup. Four separate test section sizes were used in the experiments. Two test sections had equal diameters of 4.4 cm but varied in height of the material they contained (52.0 cm and 86.0 cm). The remaining test sections had diameters of 1.3 cm and 2.2 cm with heights of 25.4 cm and 48.4 cm, respectively. A computer-activated solenoid valve allowed for a programmable time interval of bubble generation and injection along the axis of the inner cylinder just above the flat bottom surface. Combinations of bubble generation time and air supply pressure were used to control bubble size.

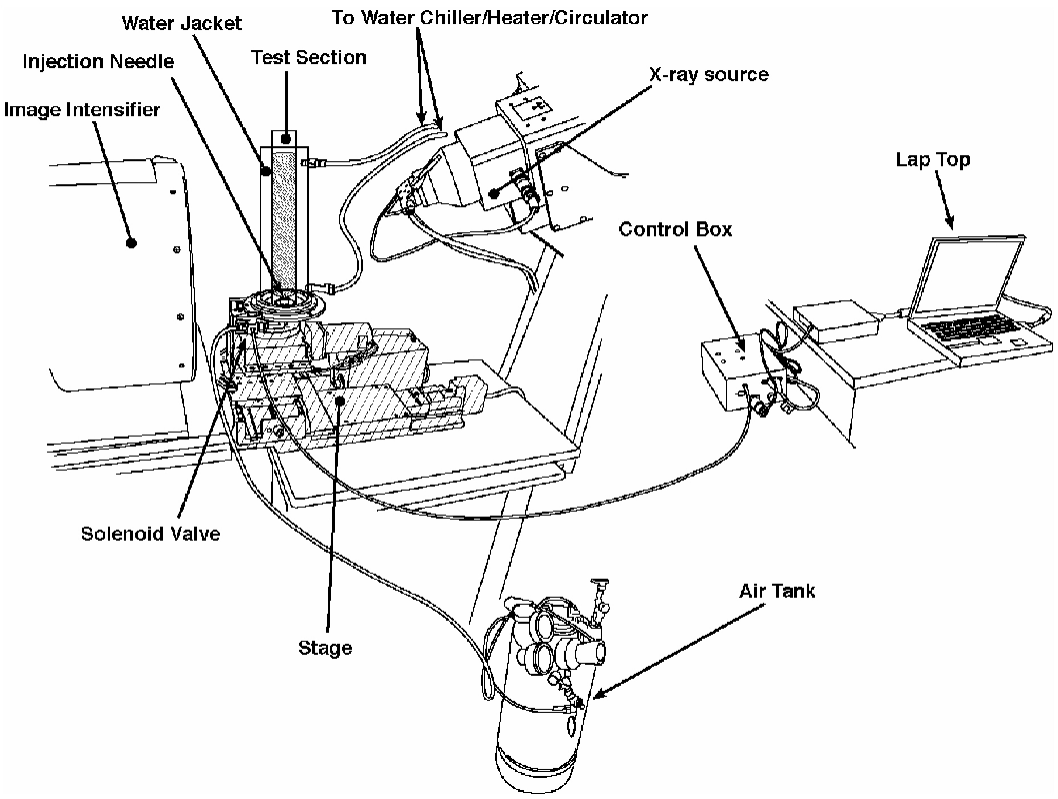

Figure 11. Experimental arrangement for studies of bubbles rising through a suspension.

Real-time radiography was used to track bubbles as they traversed the test section. Advantages of this technique include the ability to test opaque suspensions and the elimination of optical distortion that can occur with other imaging techniques.

A computer-controlled three-axis stage was used to position the bubble column apparatus relative the x-ray source. The position history of a bubble was recorded using the radiography system along with image capture software. To get sufficient spatial resolution to determine the bubble size and shape, only part of the test section was visible at one time when the longer test section was used.

Suspensions used in the experiments consisted of a disperse phase of spheres and a

continuous phase of a Newtonian liquid. Polystyrene or polymethyl methacrylate (PMMA) spheres were sieved to obtain a nominal average diameter d_s = 500 μm or d_s = 750 μm, respectively. Larger, individually ground spheres were also used.

Suspensions with disperse phase volume fractions of 0.30 and 0.50 were made with the polystyrene suspended particles (d_s = 500 and 3175 μm) in Ucon 50-HB-5100 lubricant (Union Carbide). The temperature of the experiment was adjusted until no flotation or settling was detected over several days. An additional suspension (volume fraction 0.50) was used, consisting of the polymethyl methacrylate (PMMA) spheres (d_s= 750μm) suspended in a three component fluid that is density matched to PMMA. This three component fluid consisted of 15.1% tetrabromoethane, 29.6% Ucon 75-H-90000, and 55.3% Triton X-100 by weight.

Suspensions were poured into the inner column of the bubble cylinder apparatus and allowed to sit for several hours until the temperature, as measured with a probe, was uniform throughout the inner column to ± 0.2C. Bubbles were then injected into the column on a slow, but continuous, basis and allowed to rise freely through the suspension. The bubbles were generated at sufficiently large time intervals to allow enough distance between bubbles to avoid any bubble to bubble interactions. Image sequences were captured of one or two bubbles, then the suspension was stirred to allow different microstructures to be sampled, but not so vigorously as to introduce air bubbles into the suspension.

The path of each bubble meandered, presumably highly influenced by the presence of the suspended particles. Figure 12 shows a representative reconstructed path, which is a projection into two dimensions of a three-dimensional trajectory. The shape and size of this projection could be measured, and the deformation of the bubble could be monitored.

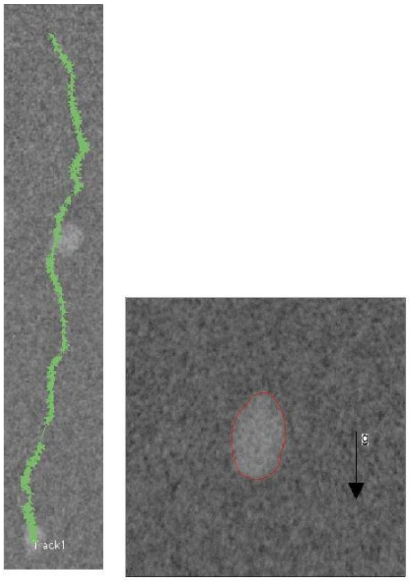

Figure 12. Left: Reconstructed path of the centroid of a bubble traveling through a suspension of 500-micron particles (50% by volume). Right: close-up of an x-ray image of the bubble.

Typically five bubbles were tracked for each suspension along the full length of the test column. The velocity of the bubbles was then determined based on the positions and time intervals found during the bubble-tracking process (Fig. 12). The rise of the bubbles was then used to determine the apparent viscosity, taking into account bubble velocity, size, and shape (Mondy et al., 2008). During experiments, effects of several factors upon the flow were considered.

The height of the contained suspension appears to have a notable effect, especially for higher volume fractions of particles. Figure 13 shows the results for bubbles rising in two Newtonian suspending liquids, either Ucon 50-HB-5100 or the three component system, with no suspended particles present. The liquids are held in a cylinder with diameter D = 4.4 cm and height L = 52 cm. These measured viscosities as a function of the distance Z from the bottom of the cylinder are derived from the average of five bubbles and are also compared to the

measurements of a similar three component fluid held in a cylinder with D = 3.7 cm and L = 83.6 cm.

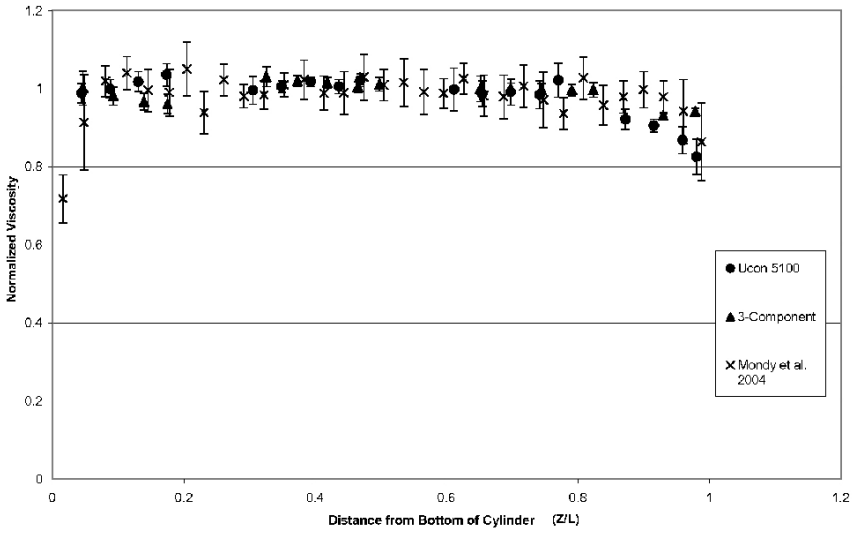

Figure 13. Bubble behavior in Newtonian fluids used in suspension experiments.

To compare the viscosities found in these experiments, each viscosity measurement is normalized by the mean viscosity of that fluid obtained by averaging the values obtained with $0.2 < Z/L < 0.7$. The bubbles achieve a steady-state velocity within the first measurement zone of height 0.5D using the x-ray system (Fig. 11). As they come within about 2D of the top (4D for the earlier data), they accelerate by about 10 to 20 percent.

In concentrated suspensions, the bubbles experienced added resistance attributable to the presence of the cylinder bottom. Figure 14 shows that in the suspension with a volume fraction of particles of 0.50, a bubble does not reach a steady velocity until about 14D. As the volume fraction of solid particles decreases, the end effects become less dramatic, and bubbles achieved steady state within 4D when the volume fraction equals 0.30. Here, each set of experiments tested 500 μm suspensions in 4.4 cm diameter cylinders. Again the points indicate averages over

measurements for five bubbles. The measured viscosity has been normalized by the steady-state viscosity for each suspension to emphasize the end effects. The actual measured viscosity varies dramatically with volume fraction.

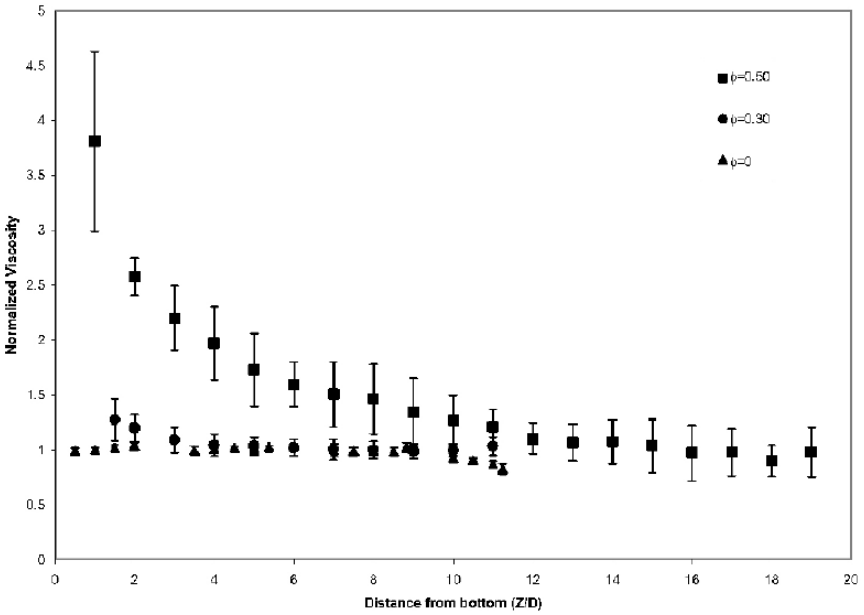

Figure 14. Viscosity profiles normalized by the steady-state viscosity for suspensions with 500-micron polystyrene spheres at volume fraction $\phi = 0$, 0.30, and 0.50.

Other factors considered were effects of the size of suspension particles on the end effects and the bubble rise velocity (Mondy et al., 2008). Results show that bubbles travel faster than one would expect from results, say, of falling-ball rheometry of similar suspensions, but this can be attributed to the fact that, unlike a heavy rigid sphere falling through a suspension, a bubble is deformable and can “squeeze” through narrow spots, producing less disruption among the suspended particles.

2.3. Experiments with batch sedimentation in geometries containing obstacles Experiments with batch sedimentation of non-colloidal particle suspensions (Rao, Mondy, and Altobelli, 2007) were conducted using with nuclear magnetic resonance flow visualization. The experimental method gives particle volume fraction as a function of time and position in three distinct geometries with particles that are heavier and lighter than the suspending fluid, depending on the experiment: sedimentation in a cylinder with a contraction; particle flotation in a horizontal cylinder with a horizontal rod; and flotation around a rectangular inclusion. Secondary flows appear when a region of higher density fluid is above a lower density fluid. The secondary flows result in particle inhomogeneities, Rayleigh–Taylor-like instabilities, and remixing.

NMR imaging can be used to study hindered settling, and also to study interfacial broadening. NMR measurements of the liquid fraction as a function of the vertical coordinate y and time t help quantify the hindered settling function. While earlier experiments using this technique relied on 1-D imaging of flow geometries with constant cross-sectional area, the experiments conducted as a part of this project use 2-D imaging to visualize particle motion in more complex systems.

The NMR imaging experiments were performed in a 1.89 T horizontal-bore, superconducting magnet equipped with shielded gradient coils (Magnex, Inc., Boston, MA) and controlled by a Tecmag (Houston, TX) Libra. The r.f. probe was a custom-built high-pass birdcage[1]. Spin echo, spin warp imaging[2] was performed with an echo time of 4 ms and repetition times of 50–100 ms. Since these repetition times are shorter than longitudinal (or spin-

1 Watkins JC, Fukushima E. The highpass birdcage coil for NMR. *Review of Scientific Instrumentation* 1988; **59**:926–929.
2 Callaghan PT. *Principles of Nuclear Magnetic Resonance Microscopy*. Oxford University Press: New York, 1991.

lattice) relaxation time T1, low-angle pulses were used for excitation, and spoiling gradients were applied during the recycle time. Single vertical slices were collected on resonance, and the imaging gradients were all less than 2G/cm.

A quiescent settling experiment was carried out in a cylinder with a contraction roughly two-thirds of the way up to investigate the effect of a horizontal obstruction on particle settling. The geometry and dimensions can be seen in Fig. 15. The suspension was made of PMMA particles in a suspending fluid composed of 22% water and 78% glycerol. The glycerol solution was formulated such that the PMMA particles had a slightly higher density than the suspending fluid, and would settle out relatively slowly.

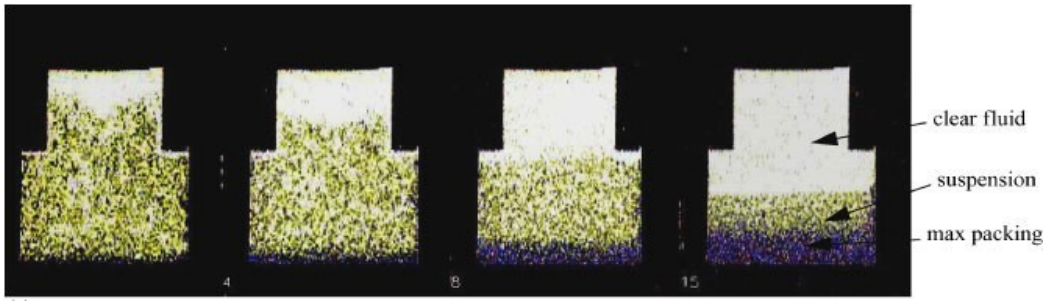

Figure 15. Particles settling in a cylinder with a contraction for a 0.192 volume fraction of 0.0397 cm radius PMMA particles in glycerol/water suspending fluid. Particles are slightly heavier than the fluid. NMR imaging shown at times $t = 105,\ 175,\ 315$, and 560 s.

The NMR imaging shows results where individual particles cannot be resolved, but the overall suspension behavior is revealed. Initially, we get a clear zone forming underneath the horizontal surfaces and particles settling on the bottom of the container. Over time, the suspension–pure fluid interface becomes V-shaped near the center of the cylinder. The final distribution of particles is also concave up. Although still images cannot capture the movement, a video produced from the NMR images clearly shows recirculation occurring in the upper portion of the container.

The next experiment investigated quiescent particle flotation in a horizontal concentric wide gap Couette cell filled with a 96% glycerol, 4% water solution. The goal was to determine the effect of a circular obstruction on settling behavior. The particles are slightly less dense than the suspending fluid, causing them to float. The Couette geometry can be seen in Fig. 16. The inner rod is one-fourth the size of the outer cylinder. Both are stationary throughout the experiment.

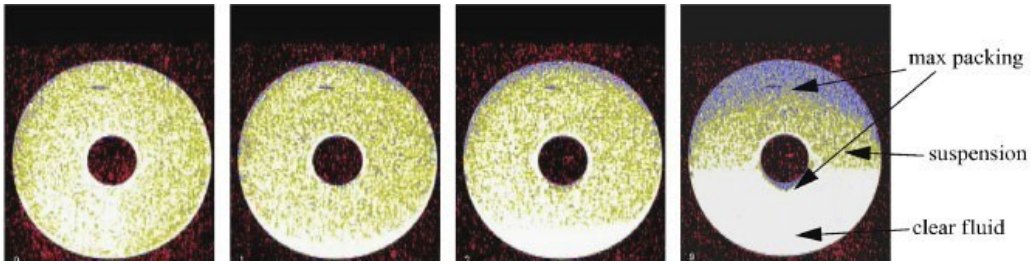

Figure 16. Results for 0.20 volume fraction PMMA particles suspended in a glycerol/water solution. Particles are floating in a horizontal Couette apparatus. Zones of maximum packing are seen at the top of the cylinder and beneath the inner cylinder. NMR imagingshows times $t = 68$, 204, 340, and 1156 s.

The results from the NMR imaging show that the suspension is initially well mixed and homogeneously distributed. Regions of maximum packing are shown in purple, white shows the pure fluid, and yellow shows the suspension. Over time, particles pile up
at the top of the container and below the rod, with clear fluid zones occurring above the rod and at the bottom of the Couette. We observe evidence of the instabilities seen in the simulation, since we can see low-concentration areas in the suspension similar to the blobs of pure fluid coming off the top of the rod. The final distribution of particles shows all particles settling at the top of the Couette with clear fluid below.

Finally, we considered particle flotation in a cylinder with a rectangular inclusion. The inclusion is actually another cylinder, when seen in a 2-D axisymmetic slice, looking like a rectangular void surrounded by fluid. The geometry and dimensions can be seen in Fig. 17. The particles were glass microballoons (GMBs), which have a very low density. The suspending fluid used is 50-HB-500 Ucon lubricant, which has a density similar to water making the particles float. The initial volume fraction is almost 40%.

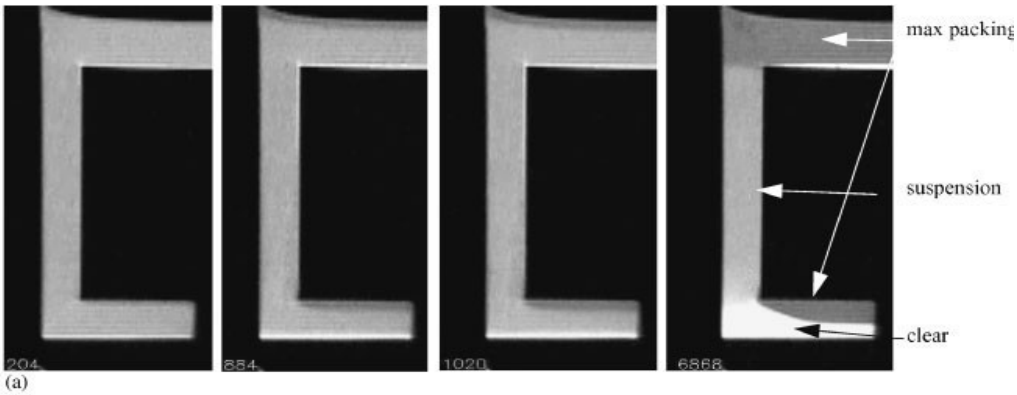

Figure 17. Particle flotation around a rectangular inclusion for 0.396 volume fraction of GMB in Ucon lubricant: volume fraction profiles as a function of time. Time stamp indicates elapsed time. NMR imaging at $t = 204,\ 884,\ 1020$, and 6858 s.

The NMR imaging shows that the suspension starts off well mixed. After 884 s, we see a clear layer forming above the inclusion and at the bottom of the container. Zones of maximum packing can be seen below the rectangle and at the top of the container. We can see some graininess that could be associated with streams of material remixing back into the suspension. This streaming phenomenon is much easier to see when the images are viewed dynamically as a movie. Similar streaming trends continue at 1020 s. The final frame, 6868 s, shows that the top instability is gone and only the bottom instability remains.

3. Numerical modeling

Interaction between our modeling effort and experiment pursued two goals. First, we used experimental results for benchmarking. Second, we used computational analysis to gain additional insight into the physics of the flow phenomena observed experimentally. In this section, we begin with the description of our progress in developing numerical methods, and then will discuss modeling results for several problems.

3.1. Numerical methods

3.1.1. Studies of the microscale breakdown of lubrication theory

At a sufficiently small scale the force that acts between two approaching (or receding) surfaces must display strong signs of a breakdown of the hydrodynamic lubrication force. The latter exhibits an unphysical divergence as the gap size shrinks to zero. In addition, it applies a no-slip boundary condition that previous molecular dynamics simulations have shown to become inadequate at the small scale. It is also well known that at the nano and molecular scale there exist solvation forces that can be quite pronounced and moreover at these small length scales fluctuations (in density, stress, forces etc) become significant. To investigate the details of the breakdown of lubrication theory and the interplay between solvation forces and hydrodynamic forces we have performed preliminary molecular dynamics calculations of a sphere moving through a molecular fluid near a wall.

3.1.2. Studies of particle-scale coupling methods

We have examined mathematical coupling methods at the particle scale which accurately account

for hydrodynamic effects under near-contact and full-contact conditions. In anticipation of supporting a modeling capability that deploys a distributed Lagrange Multiplier approach (DLM) to couple particle and fluid mechanics as a complimentary approach to the more traditional boundary element methods, we have examined the breakdown of continuum finite element/overset Langrangian solid coupling. More specifically, we are deploying a unique approach that allows for Lagrangian mechanics in the particles to be coupled in a Newton-Raphson framework with an incompressible flow solver using the mortar finite element method and distributed Lagrange multiplier constraints.

3.1.3. Coarse-grained rigid blob method

We have performed work on coupling the coarse-grained rigid blob method to the boundary element technique. The coarse-grained method will be performed on the fly in a small box determined by the boundary element at the point of closest approach of the two approaching spheres. The boundary conditions on the coarse-grained molecular dynamics, for rigid blobs representing the fluid between the spheres, will be determined by the velocity fields obtained in the previous iteration of the boundary element method. The velocity field will be used to set a gradient of velocities across the box at the point of closest approach and the simulation will be performed until the system equilibrates. At that point, the tractions of the surface of the spheres will be calculated and passed back to the boundary element method to carry out the next iteration.

3.1.4. Microscale/mesoscale coupling

Linking recent progress in molecular- and nano-scale science to progress in the ability to accurately model suspension flows at the macroscale is an important challenge for several energy-related technologies. The numerical investigation is based on a novel multiscale approach that seamlessly couples micro/nanoscale and mesoscale simulations using an "equivalent force" approach and couples mesoscale and macroscale simulations using a substructuring approach. Current continuum-level simulations of suspension flows typically rely on models that account for irreversibilities in the systems in an *ad hoc* fashion with empirically determined adjustable parameters having little or no physical basis. As a result, there is no "universal" set of these parameters, and hence, they must be adjusted for different particle types and flow geometries. In contrast, the proposed research will rely predominantly on a first-principles approach in order to develop a predictive high-fidelity simulation capability.

3.1.5. Traction-corrected boundary element method (TC-BEM)

This work focuses on development of robust numerical simulation capabilities for suspensions of small solid particles in liquids, incorporating effects spanning diverse time and length scales. In the current research, a new method is developed to incorporate the near field effects into the boundary element method. Rather than working with lubrication forces as done previously, asymptotic solutions have been derived for traction field in the interstitial regions between particles. The calculation of the traction unknowns, for a single boundary element centered around the point of nearest contact, is based on the relative motion of the two partilces in terms of the asymptotic traction solutions. In this way, the system remains fully coupled incorporating

both the boundary element representation for alll other elements along with the near field asymptotics.

3.2. Modeling of specific problems of interest

In this section, attention is given to not just to details of modeling specific problems, but to experimental validation and to the physical insights that the numerical results provide.

3.2.1. Modeling of particle-pair interaction

We have examined two-particle geometries with a user-prescribed particle squeezing flow and compared the integrated particle stress (force) with analytical solutions in a creeping flow regime. We have found (not surprisingly) that agreement is good at separations of order of one particle diameter, but as the gap closes to nanometer length scales the predicted singularity in the lubrication stress (force) is grossly under-predicted.

We have also begun work on directly coupling mesoscopic and microscopic simulations. Initial simulations have been performed for two spheres approaching along their lines of centers through a specified force. Based on the level of mesh refinement, the separation at which the numerical results diverge from the analytical solution has been determined. An analytic solution for the traction field on the surface of the particles has been developed based on the work of Brenner for the velocity and pressure fields (Chemical Engineering Science, Vol. 16, 1961). This work has provided the most accurate multibody simulations available.

Using TC-BEM (Section 3.1.5), we obtained the quantitative agreement of the self-diffusivities with the analytic model for two rough spheres. By combining theoretical analysis

with hydrodynamic simulations, TC-BEM is able to correctly model both the far field macroscale interactions and the near contact microscale interactions (Zhu and Ingber, 2008).

The numerics show that there is a net migration of the center of gravity of a pair of rough spheres suspended in a nonlinear shear flow towards the low shear rate region of the flow. This migration increases with the nonlinearity of the flow field (characterized by a nonlinearity parameter described by Ingber et al., 2008) and with particle roughness, in agreement with experiment (Figs. 18, 19). The nonlinearity parameter is defined as $(d\nabla\dot{\gamma})/\dot{\gamma}$, where $\dot{\gamma}$ is the local shear rate.

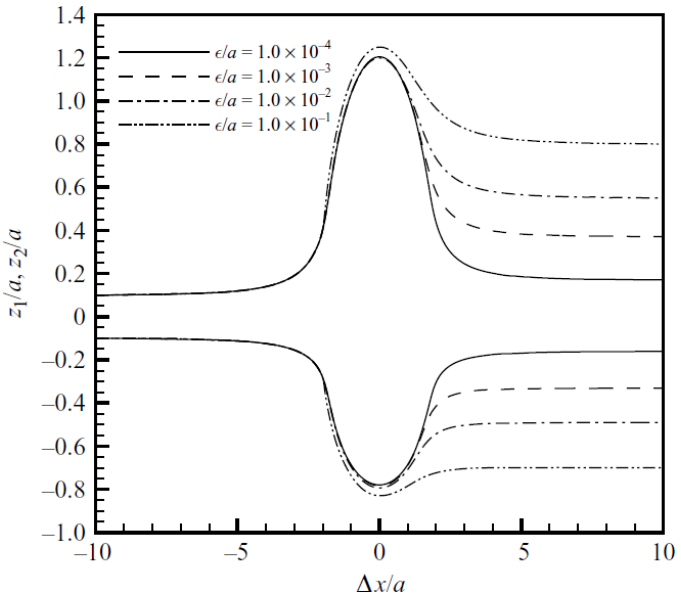

Figure 18. Typical TC-BEM-simulated trajectories in the shear plane of two rough spheres suspended in a nonlinear shear flow with initial positions (−5.0, 0.05, 0.1) and (5.0,−0.05,−0.1) and nonlinearity parameter set to 1. Irreversibility increases with surface roughness.

The migration diffusivity coefficient measures the variance of the location of the particle-system center of gravity caused by the two-particle interactions. Unlike the self-diffusivity coefficients,

there is an associated directionality of the migration towards the low-shear-rate region of the flow field.

For particle-pair interaction in Couette cell shear flow (Section 2.1, Popova et al., 2007), modeling using TC-BEM (Section 3.1.5) was conducted both to see if the particle migration can be faithfully reproduced numerically and to provide a better understanding of its physical causes. Consider a sequence of snapshots of two particles suspended in a shear flow with a fixed center of gravity but with a variety of surface-to-surface separations.

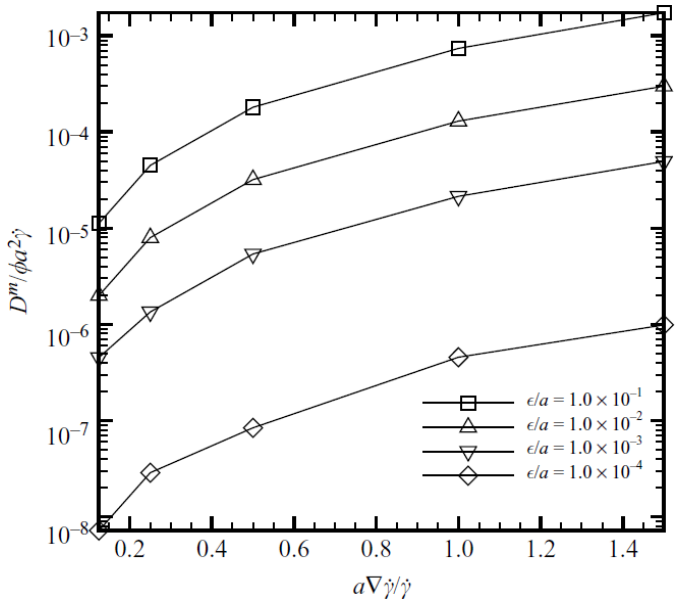

Figure 19. The migration diffusivity coefficient, D^m divided by $\phi a^2 \dot{\gamma}$, where ϕ is volume fraction and a is particle size, as a function of the nonlinearity parameter, for various particle rougnesses. D^m increases both with the particle roughness and the nonlinearity parameter.

In our numerical simulation, the center of gravity of the particle pair migrated toward the low-shear-rate region of the flow field. We took snapshots, perturbing the particles inward toward each other along the line of centers. A plot of the velocity of the center of gravity V_{ave} as a

function of separation δ/d, d being the particle size, is shown in Fig. 20.

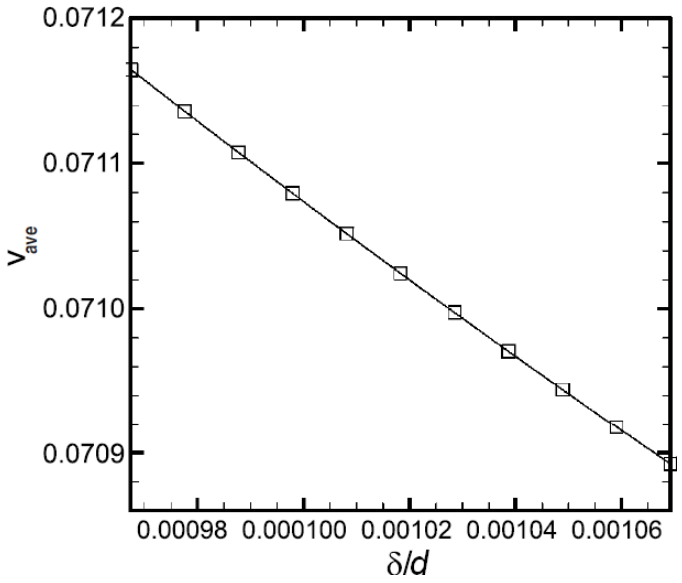

Figure 20. Average dimensionless velocity of the center of gravity of a pair of particles in nonlinear shear flow as a function of particle separation δ/d (numerical simulation results).

The migration velocity is seen to decrease with increasing separation. This simulation illustrates why rough particles migrate toward the low-shear-rate region of the flow field. If the particles were perfectly smooth, then the particle trajectories would be perfectly symmetric upon approach and separation. At a certain location upon approach, the particles would move toward the low-shear-rate region of the flow field with a given speed. At the symmetric point during separation, the particles would be exactly the same distance apart, and hence the particle pair would move toward the high-shear-rate region of the flow field with the exact same speed as upon approach. Hence, after separation, there would be no net migration of the particle pair. However, for rough particles, the distance between the particles on separation is greater than on approach, and hence the speed at which the particles move toward the low-shear-rate region on approach is faster than

the speed at which the particles move toward the high shear-rate region on separation. Therefore, the net effect is the observed migration of the particle pair toward the low shear-rate region of the flow field.

How would this result compare with particle migration according to existing rheological models? If the model uses a repulsive interactive force, finite normal stress would arise in particle interaction. Hence, using the well-known suspension balance model of Nott and Brady[3] , particle migration would also ensue. The argument for the finite normal stress, however, relies on the presence of multiple interacting particles, and would not necessarily apply to a two-particle system, whereas in our experiments, the effects of the nonconstant shear rate are the apparent cause of the migration of the particle pair. Moreover, the suspension balance model predicts the particle migration rate to scale as the particle radius squared, like the particle self-diffusivity. Prior experiments already rule out the possibility that this scaling is realized. Our experimental results strongly suggest that rheological models for suspension flows can be improved by giving more consideration to the nonlinearity of the flow field.

3.2.2. Modeling of chaotic behavior in particle triplets.

To model the interaction of three particles in shear flow (Section 2.1), TC-BEM method described in Section 3.1.5 is employed to solve the governing Stokes equations. The boundary element methods transform Stokes equations into Boundary Integral Equations (BIEs) by considering a weighted residual formulation with the fundamental solutions for Stokes equations, thus leading to the reduction of problem dimensionality by one. To treat the lubrication forces between nearly touching particles accurately, TC-BEM combines the analytical asymptotic

3 P. R. Nott and J. F. Brady, J. Fluid Mech. **275**, 157 1994.

solution in the interstitial regions with BIEs. Surface imperfection on spherical surfaces is then introduced as the irreversible source for particle trajectories and is represented by a non-locked roughness model. The normal relative motion of the particles is restricted when the separation between particles becomes less than the specified sphere roughness. The employment of TC-BEM allows us to correctly predict the trajectories of particles suspended in nonlinear shear flows and to perform accurate analysis of irreversibility.

Moreover, the chaotic behavior of the particle triplet observed in experiments is faithfully reproduced. Subsequently the phase portrait of the three-particle system (Fig. 21) can be analyzed numerically by conducting multiple numerical runs with small perturbations applied to initial conditions of particles. The investigation also reveals that particle roughness affects the three-particle system discontinuously, unlike the two-particle system.

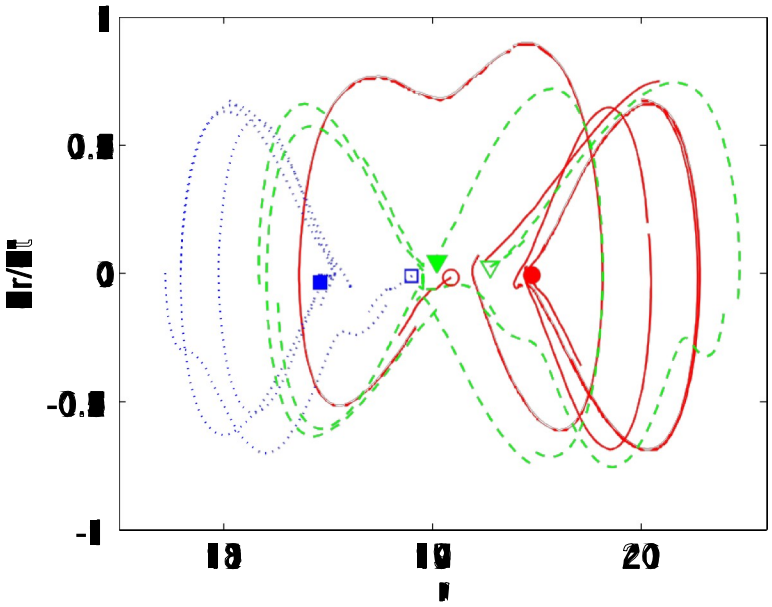

Figure 21. Phase portrait in the (r, r') plane of a three-particle system in shear flow. Butterfly- shaped trajectories indicate particles changing places with each other.

3.2.3. Modeling of surfactant effects on drop coalescence

For problems involving the interaction and possible coalescence of bubbles or drops in a flow, the critical feature is the presence of a very thin film between the drops or bubbles, the dynamics of which is critical to determining whether coalescence takes place or not. From a computational perspective, the issue is the 3-5 order of magnitude difference in length scale between the drops and the thin film; the fact that the thin film is unknown in shape though the evolution of this shape is critical to the overall process; and the fact that the thin film must achieve length scales of order 100 angstrroms before van der Waals forces become significant and lead to film rupture. At this length scale, many of the classical assumptions of continuum mechanics begin to break down.

We have worked on completing very careful and accurate solutions of the film thinning process for head-on axisymmetric collisions based upon a classical continuum model, with van der Waals forces incorporated via a disjoining pressure approximation.

We have developed an extended version of the disjoining pressure model for van der Waals forces. The classic theory, used by all previous investigators, is valid for a pair of parallel flat surfaces of infinite extent. In this simplest "unretarded" form, this model assumes that the disjoining pressure is

$$\Pi = -\frac{A_H}{6\pi h^3}$$

where A_H is the Hamaker constant and h is the uniform film thickness (which is assumed to be the local film thickness when this formula is applied to non-parallel interfaces). We have extended this theory to incorporate corrections for the situation in which the interfaces are not parallel and also exhibit local curvature,

$$\Pi = -\frac{A_H}{24\pi h^3}\left(4 - 3h_x^2 + 3hh_{xx}\right)$$

This correction to the physical model is not difficult to incorporate into the numerical algorithm, but is very important for accurate predictions for this class of multiscale problems (Dai, Leal, and Redondo, 2008).

The computations still require a relatively sophisticated adaptive remeshing scheme to achieve adequate resolution within the thin film region, while maintaining reasonable computational times. More work will be required to extend these calculations to a fully 3D configuration. The parameter values were chosen to correspond to real fluids, where we have experimental data available. Comparisons with this data shows reasonable qualitative agreement, but with quantitative details and even some scaling behavior (for example, with drop size) that do not agree well. We believe that this is because of a breakdown in various aspects of the continuum model that we have used. To resolve this problem, one must incorporate molecular information into the simulation of the thin film dynamics.

A computational algorithm has been developed to simulate the effects of surface active additions on the axisymmetric ("head-on") drop collision, thin film drainage and rupture process. This involves a composite numerical scheme – with the BI-based scheme with mesh refinement for the viscous flow, and a finite-element formulation for the surfactant transport problem. This scheme produces very accurate solutions, but is significantly slower than the code without surfactant, and we have only been able ("willing") to obtain comprehensive results for the numerically simple case when the viscosity ratio λ=1. The results include a new understanding of the mechanisms by which surfactants inhibit coalescence (Dai and Leal, 2008).

Consider axisymmetric head-on collision and coalescence of a pair of equal size

Newtonian (though polymeric) drops in a Newtonian (though polymeric) suspending fluid, in the presence of an insoluble (polymeric) surfactant. For simplicity in the analysis, the viscosity of the suspending fluid is assumed to be the same as the viscosity of the drops. Interfacial dynamics for Stokes flow can then be represented by a boundary integral of the unknown surfactant concentration function and its derivatives,

$$\mathbf{u}(\mathbf{x}_0) = \mathbf{u}^{\infty}(\mathbf{x}_0) - \frac{1}{8\pi\, Ca} \int \mathbf{G}(\mathbf{x}, \mathbf{x}_0) \cdot \left\{ \nabla_s \gamma(\Gamma) + \left[\Pi - \gamma(\Gamma)(\nabla \cdot \mathbf{n}) \right] \mathbf{n} \right\} ds(\mathbf{x}) \quad (1)$$

where $\mathbf{G}(\mathbf{x}, \mathbf{x}_0)$ is the free space Green's function while the whole term in the curly bracket is the stress difference along the interface. The stress difference is induced by the capillary pressure

$\gamma(\Gamma)(\nabla \cdot \mathbf{n})\mathbf{n}$, the Marangoni stress $\nabla_s \gamma(\Gamma)$, and the disjoining pressure $\Pi\mathbf{n}$ accounting for the van der Waals interactions at small scales. $Ca \equiv \mu G R / \gamma$ is the capillary number, which measures the relative magnitude of viscous to capillary forces, and $\mathbf{u}^{\infty}$ is the external flow. The drop shapes and positions are updated based upon the kinematic condition using the velocity calculated from equation 1.

With the presence of surfactants, the interfacial dynamics is fully coupled with the surfactant transport equation 2 that is solved via a Galerkin finite element method. The interfacial surfactant concentration is constructed from a set of Lagrangian quadratic basis functions defined on the moving mesh determined by the interfacial dynamics, e.g., equation 1.

$$\frac{\partial \Gamma}{\partial \tau} - \mathbf{U}_{\mathbf{ref}} \cdot \nabla_s \Gamma + \nabla_s \cdot (\Gamma \mathbf{u}_s) = \frac{1}{Pe_s} \nabla_s^2 \Gamma + \Gamma(\mathbf{u} \cdot \mathbf{n}) \nabla \cdot \mathbf{n} = 0 \quad (2)$$

Here $Pe_s \equiv G R^2 / D_s$ is the interfacial Péclet number, the ratio of convective to diffusive flux and

$\mathbf{U}_{ref}$ accounts for the moving reference frame. A time-marching scheme is employed to exchange data between equation 1 and 2 for a convergence of both equations. Figure 22 shows the collision between two equal-sized drops with a uniform initial surfactant distribution in an axisymmetric, biaxial extensional flow. A surfactant gradient is built up along the interface and the interfacial dynamics is completely different from that of the clean interface due to the Maragoni stress induced by the surfactant gradient.

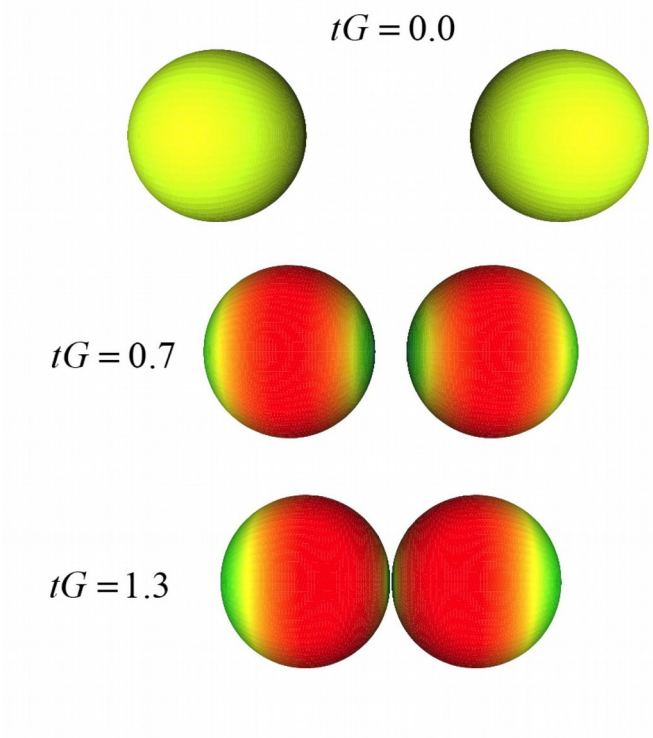

Figure 22. Collision between two equal-sized drops with a uniform initial surfactant distribution along the center line in an axisymmetric, biaxial extensional flow (red: higher surfactant concentration; blue: lower surfactant concentration).

Our benchmark results show that during coalescence, the interface in the thin gap actually exhibits a significant degree of mobility. This explains, at least to certain degree, the fact that the

scaling behavior based on the assumption of a completely immobilized interface is not in agreement with recent experimental measurements. The unexpected new result is that the role of Maragoni effects on the coalescence process does not occur via immobilization of the interface within the thin gap region, but rather due to its effects on the hydrodynamics outside the thin film. In particular, Marangoni streses immobilize the drop interface outside the thin film and this increases the total external hydrodynamic-force that pushes the drops toward each other. This, in turn, increases the degree of flattening and dimpling of the thin film, and it is primarily this change that slows the film drainage process and thus increases the required drainage time prior to coalescence.

3.2.4. Water in a slit pore

One of the relevant microscale aspects of liquid/particle interaction is the behavior of fluid confined in a pore, e.g., near the wall of the particle. of the With an extension of the Bell−Salt lattice model of water a study of water confined in a slit pore has been conducted (van Swol, Liu, and Monson, 2008). Wall−fluid interactions are chosen to be qualitatively representative of water interacting with a graphite surface. We have calculated the bulk vapor−liquid phase coexistence for the model through direct Monte Carlo simulations of the vapor−liquid interface. Adsorption and desorption isotherms in the slit pore were calculated using grand canonical ensemble Monte Carlo simulations. In addition, the thermodynamic conditions of vapor−liquid equilibrium for the confined fluid were determined. Our results are consistent with recent calculations for off-lattice models of confined water that show metastable vapor states of confined water persisting beyond the bulk saturation conditions, except for the narrowest pores. The results are similarly consistent

with recent experiments on water adsorption in graphitized carbon black.

3.2.5. Large sphere near a flat surface

Consider a large sphere moving toward a flat substrate, or two large spheres moving toward each other. Classical molecular dynamics simulations of these problems were conducted to investigate hydrodynamics at the molecular scale (microscale, in the terminology of our framework). The study also addresses a familiar question underlying force microscope measurements: how does one properly separate hydrodynamic forces from hydration forces? A new decomposition approach we developed allows to extract the static and dynamic components from approaching- and receding-force curves that are obtained from simulations or experiments (Fig. 23), to compare the dynamic force contribution to hydrodynamic predictions, and to assess the effects of surface roughness.

3.2.6. Suspension models for a thixotropic fluid

Thixotropy (shear thinning) is a property possessed by certain gels or fluids that are thick (viscous) under static conditions, but will flow (become thinner, less viscous) over time when shaken, agitated, or otherwise stressed. They then take a fixed time to return to a more viscous state.

We have evaluated a practical implementation of several thixotropic rheological models for a prototypical industrial application (Grillet et al., 2009). We have studied the ability of the models to predict both steady and transient rheology of a suspension of alumina particles and the suitability of those models for full transient finite element calculations.

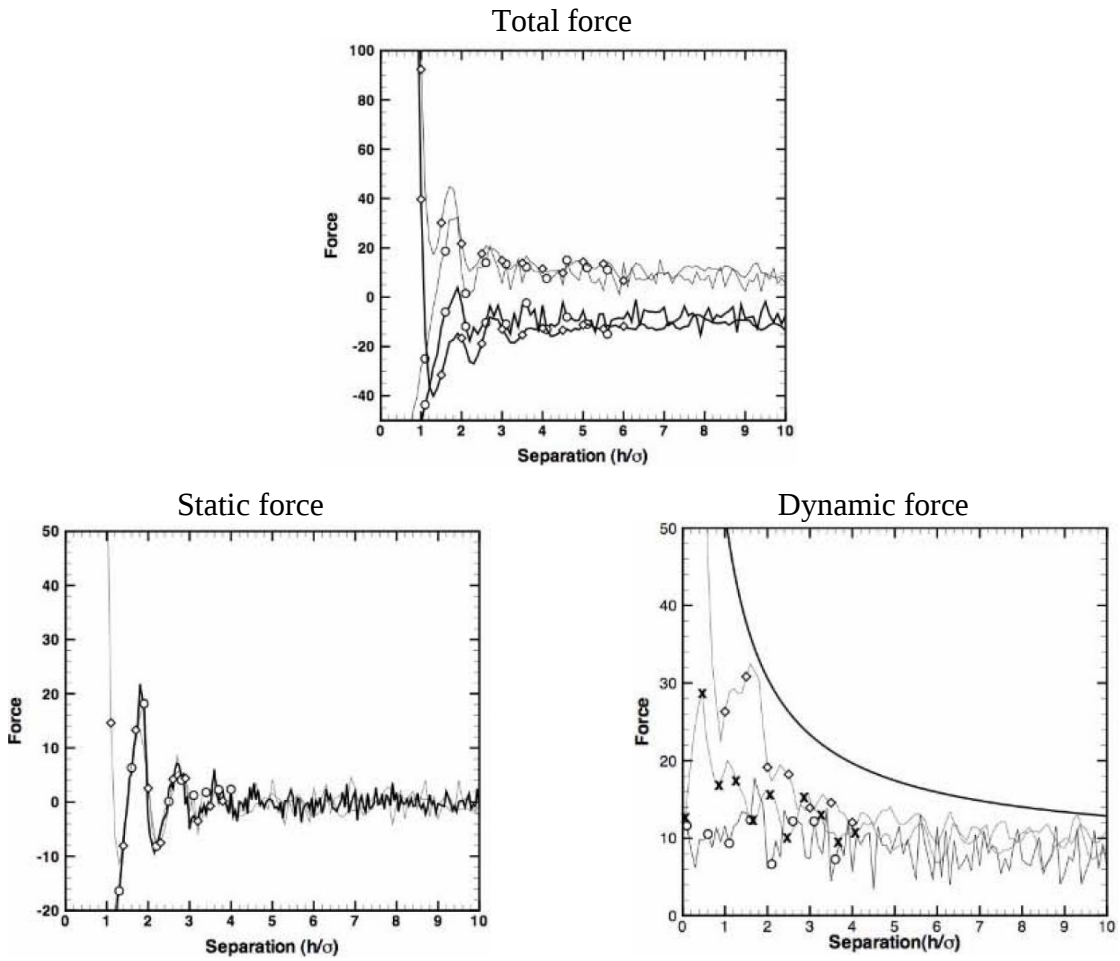

Figure 23. Results of molecular dynamics simulation of a sphere approaching to or receding away from a structured atomistic wall (diamond). Circles denote the case when instead of a sphere and a wall, two identical spheres approach / recede from each other. Top – total force. Thin curves correspond to approaching sphere(s), thick – to receding sphere(s). Bottom left – thin curve shows static force exerted onto a smooth sphere obtained by decomposition of the same data, thick curve is solvation force between two (stationary) spheres. Bottom right – dynamic force (thin curve), again resulting from decomposition of the same data. Crosses represent the dynamic force between a smooth sphere of radius R=4 and the wall, solid curve shows the continuum hydrodynamics result.

The constitutive models for thixotropic materials examined include the Carreau-Yasuda model and first and second-order indirect structure models.

While all of these models were able to predict the shear-thinning behavior of the steady viscosity, the first and second-order structure models were also able to capture some aspects of the transient structure formation and fluid history. However, they were not able to predict some more complex transient behavior observed in step shear experiments. For most thixotropic suspensions, the time constant required to form structure is longer than the time constant to break it down. For this suspension, the time constant at a given shear rate was also dependent on the previous shear rate. If the previous shear rate was high, the time required to reach equilibrium was longer than if the previous shear rate was lower. This behavior was not captured by the simple initial structure dependence in the previous models.

By adding an additional dependence on the initial suspension structure, the prediction of the transient rheology was substantially improved while maintaining an excellent agreement with the steady shear viscosity. Finite element results are presented for extrusion of a suspension to form a fiber. This model two-dimensional problem contains many of the same complexities as practical three-dimensional mold filling simulations (i.e., nonviscometric and mobile free surface). Our results show that these direct structure models exhibit oscillations near the stick-slip point in finite element calculations similar to many polymeric constitutive equations, but are otherwise suitable for implementation in complex industrial modeling applications.

3.2.7. Modeling sedimentation in geometries containing obstacles

Continuum-level numerical modeling of particle migration is validated using the NMR

suspension-study data (Section 2.3, Rao, Mondy, and Altobelli, 2007). A finite element method is used to discretize the equations of motion, including an evolution equation for the particle volume fraction and a generalized Newtonian viscosity dependent on local particle concentration. The diffusive-flux equation is based on the Phillips model (*Phys. Fluids A* 1992; **4**:30–40) and includes sedimentation terms described by Zhang and Acrivos (*Int. J. Multiphase Flow* 1994; **20**:579–591). Results of modeling are compared with NMR images of settling suspension flows in several geometries (Fig. 24).

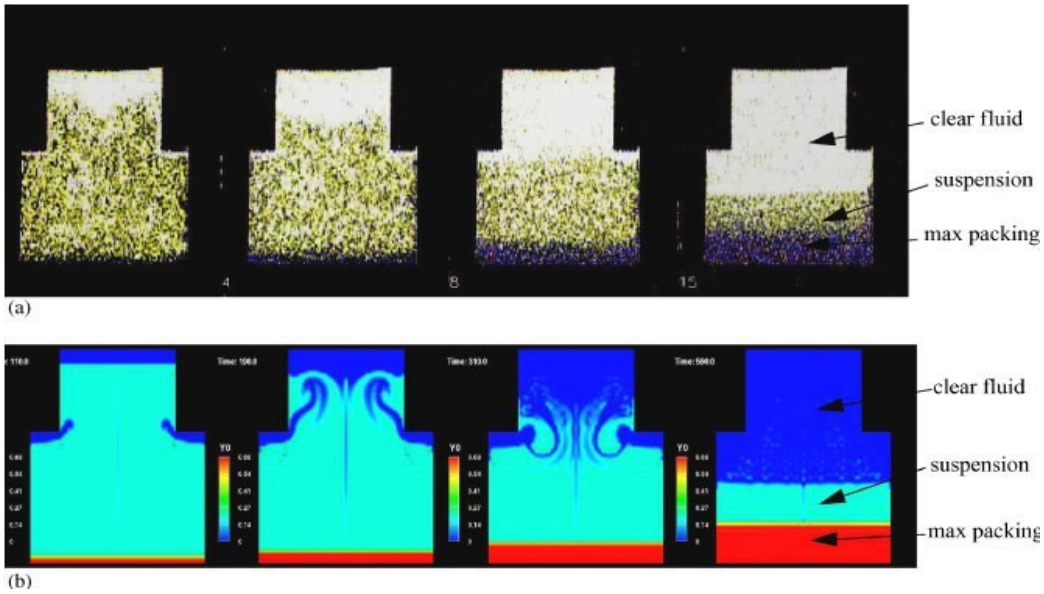

Figure 24. Particles settling in a cylinder with a contraction for a 0.192 volume fraction of 0.0397 cm radius PMMA particles in glycerol/water suspending fluid. Particles are slightly heavier than the fluid: (a) NMR imaging at times $t = 105,\ 175,\ 315$, and 560 s and (b) finite element simulations at $t = 110,\ 190,\ 310$, and 590 s.

For the example shown in Fig. 24 (cylinder with a contraction), in the finite element simulations, we see clear fluid regions developing at the top of the cylinder and directly under the contraction.

A zone of maximum packing forms at the bottom of the container as particles pile up. Over time, the clear layers under the contraction release a bubble of fluid that moves down the gravimetric potential towards the top of the cylinder. Once the blob of pure fluid reaches the suspension–pure fluid interface near the top of the container, its momentum begins to deform it, causing the interface to bulge upward. The layer of high-density suspension over a lower-density blob of pure fluid causes a Rayleigh–Taylor instability[4], which results in remixing and recirculation near the suspension–pure fluid interface. This causes pure fluid to move downward and suspension to move upward, counter to their natural inclination. Once the interface moves below the obstruction, the settling becomes monotonic. However, because of the instability, the final distribution of particles is slightly concave up instead of flat as it would be for settling in a cylinder without an obstruction. While the numerics are consistent with experiment, modeling reveals features not seen even with flow imaging as sophisticated as NMR.

4. Conclusions

We have experimentally demonstrated how microscale phenomena affect suspended particle behavior on the mesoscale, and how particle group behavior on the mesoscale influences the macroscale suspension behavior. Semi-analytical and numerical methods to treat flows on different scales have been developed, and a framework to combine these scale-dependent treatment has been described.

Results of our studies have been widely disseminated via publications in leading

4 Strictly speaking, this is not Rayleigh-Taylor instability proper, but its multiphase analog, which has been described only recently (Vorobieff et al. (2011). Analogues of Rayleigh-Taylor and Richtmyer-Meshkov instabilities in flows with nonuniform particle and droplet seeding. *Computational Methods in Multiphase Flow VI, A. Mammoli, and C. Brebbia, eds., WIT Press, Ashurst, Southampton, UK*, 17-28).

scientific journals and presentations at top national and international conferences. Proposals for follow-up research have been submitted.

Below we list important specific conclusions for several problems/methods/directions of interest.

TC-BEM numerical method. The traction-corrected scheme developed as the result of this research is able to correctly resolve the lubrication forces between nearly touching particles, thus enabling the accurate analysis of particles suspended in nonlinear shear flows. The method can be easily adapted for multi-modal systems, as asymptotic traction solutions for arbitrarily sized spheres have already been developed. For more general shapes, the analytic asymptotic traction solutions can be replaced by molecular simulations in the interstitial regions between particles.

Particle-pair interaction in shear flow. We have experimentally demonstrated that the effectively two-dimensional interaction of a pair of nearly spherical particles in nonlinear shear flow is irreversible. As the result of the two-particle interaction, the particle pair moves in the direction of lower shear. The extent of this motion is strongly correlated with the particle roughness. The results have been successfully used to validate a TC-BEM code.

Interaction of particle triplets in shear flow. The trend for the center of mass of the group (triplet) of particles to move in the direction of lower shear is present in this case as well. The three-particle system also manifests a greater degree of unpredictability in the sense that, without the knowledge of the particle trajectories, it is impossible to tell which particle corresponds to which when comparing their initial and final positions. The presence of a third particle greatly increases the system sensitivity to small fluctuations in the initial conditions. These behaviors are

observed even for fairly smooth (relative roughness $\sim 10^{-4}$) spheres. The results have been successfully used to validate a TC-BEM code.

Bubble rising in a suspension. Based on the behavior of a bubble rising through a suspension, apparent suspension viscosity can be assessed. This apparent viscosity of a moderately concentrated suspension (volume fraction 0.30) is insensitive to the relative sizes of the bubble and the suspended particles. Also, wall effects developed for spherical bubbles moving through single-phase Newtonian fluids approximate well the wall effects in moderately concentrated suspensions over a range of particle and bubble sizes, as shown by the ability of the rising bubble's velocity to predict the suspension viscosity measured with other rheometer types. However, in these suspensions Newtonian end effects are not valid. The bubbles are influenced by the bottom over a much greater distance than in the suspending fluid alone, and this enhancement of the end effects increases as the concentration of particles increases. The bubbles also travel faster than would be predicted in concentrated suspensions based on the expected suspension apparent viscosity as reported in the literature. The difference can be attributed to bubble deformability (e.g., compared with falling-ball rheometry).

Disjoining pressure model for van der Waals forces. It is known that the concept of the disjoining pressure between two parallel interfaces due to van der Waals interactions cannot generally be extended to films of nonuniform thickness. A formula for the disjoining pressure for a film of non-uniform thickness has been derived by minimizing the total Helmholtz free energy for a thin film residing on a solid substrate.

Selected presentations

2006

Leal, L. G., Dai, B., Hsu, A., & Yoon, Y. (2006, November). Studies of Surfactant Effects in the Breakup and Coalescence of Viscous Drops. *59th APS Division of Fluid Dynamics Annual Meeting, Tampa Bay, Florida.*

Popova, M., Vorobieff, P., & Ingber, M. (2006, November). Experimental investigation of particle interaction in Couette flow. *59th APS Division of Fluid Dynamics Annual Meeting, Tampa Bay, Florida.*

2007

Challa, S. R., Usabiaga Zabaleta, M., Ingber, M., & van Swol, F. (2007, March). Hydrodynamic Forces in the Lubrication Regime: A Molecular Dynamics Study. *APS Annual Meeting, Denver, Colorado*.

Popova, M., Vorobieff, P., & Ingber, M. (2007, July). Analysis of two- and three-particle motion in a Couette cell. *4th International Conference on Computational Methods in Multiphase Flow, Bologna, Italy.*

Popova, M., Vorobieff, P., Ingber, M., & Graham, A. (2007, November). Dissipative interactions between particles in shear flow. *60th PS Division of Fluid Dynamics Annual Meeting, Salt Lake City, Utah*.

2008

Zhu, G., Popova, M., Ingber, M., & Vorobieff, P. (2008, November). Phase portrait of irreversible low-Reynolds number flow. *61st APS Division of Fluid Dynamics Annual Meeting,*

Selected publications

2007

Liu, J. C., Monson, P. A., & van Swol, F. (2007). Studies of a lattice model of water confined in a slit pore. *The Journal of Physical Chemistry C*, *111*(43), 15976-15981.

Popova, M., Vorobieff, P., Ingber, M. S., & Graham, A. L. (2007). Interaction of two particles in a shear flow. *Physical review. E, Statistical, nonlinear, and soft matter physics*, *75*(6 Pt 2), 066309-066309.

Popova, M., Vorobieff, P., & Ingber, M. (2007). Analysis of two-and three-particle motion in a Couette cell. *Computational Methods in Multiphase Flow IV, editors: AA Mammoli, CA Brebbia, WIT Press, Southampton, UK*, 315-324.

Rao, R. R., Mondy, L. A., & Altobelli, S. A. (2007). Instabilities during batch sedimentation in geometries containing obstacles: A numerical and experimental study. *International Journal for Numerical Methods in Fluids*, *55*(8), 723-735.

2008

Dai, B., & Leal, L. G. (2008). The mechanism of surfactant effects on drop coalescence. *Physics of Fluids*, *20*(4), 040802.

Dai, B., Leal, L. G., & Redondo, A. (2008). Disjoining pressure for nonuniform thin films. *Physical Review E*, *78*(6), 061602.

Ingber, M. S., Feng, S., Graham, A. L., & Brenner, H. (2008). The analysis of self-diffusion and migration of rough spheres in nonlinear shear flow using a traction-corrected boundary element method. *Journal of Fluid Mechanics*, *598*, 267-292.

Ingber, M. S., Zabaleta, M. U., Graham, A. L., Challa, S. R., & van Swol, F. (2008, February).

On the Interplay between Hydrodynamic and Solvation Interactions. In *MULTISCALE AND FUNCTIONALLY GRADED MATERIALS 2006:(M&FGM 2006)* (Vol. 973, No. 1, pp. 919-924). AIP Publishing.

Mondy, L. A., Retallack, C., Thompson, K., Barney, J., Grillet, A., & Graham, A. L. (2008). On bubbles rising through suspensions of solid particles. *AIChE Journal*, *54*(4), 862-871.

2009

Grillet, A. M., Rao, R. R., Adolf, D. B., Kawaguchi, S., & Mondy, L. A. (2009). Practical application of thixotropic suspension models. *Journal of Rheology*, *53*(1), 169-189.

Ingber, M. S., Graham, A. L., Mondy, L. A., & Fang, Z. (2009). An improved constitutive model for concentrated suspensions accounting for shear-induced particle migration rate dependence on particle radius. *International Journal of Multiphase Flow*, *35*(3), 270-276.

Zhu, G., & Ingber, M. S. (2009). Accurate treatment of lubrication forces between rigid spheres in viscous fluids using a traction-corrected boundary element method. *Engineering analysis with boundary elements*, *33*(4), 467-473.

2010

Ingber, M. S. (2010). Combined static and hydrodynamic interactions of two rough spheres in nonlinear shear flow. *Journal of Rheology*, *54*(4), 707-718.